20

Pathways to increase reconstruction accuracy and depth sensitivity in mesoscopic fluorescence molecular tomography

© A.B. Konovalov¹, V.V. Vlasov¹, S.I. Samarin¹, I.D. Solovyev², D.K. Tuchina^{3,4}, A.P. Savitsky², V.V. Tuchin^{3,4,5}

- ¹ Russian Federal Nuclear Center Zababakhin All-Russia Research Institute of Technical Physics, Snezhinsk, Russia
- ² Bach Institute of Biochemistry, Research Center of Biotechnology of the Russian Academy of Science, Moscow, Russia
- ³ Saratov National Research State University, Saratov, Russia
- ⁴ Tomsk State University, Tomsk, Russia
- ⁵ Institute of Precision Mechanics and Control, FRS Saratov Scientific Center of the Russian Academy of Science, Saratov, Russia

e-mail: a_konov@mail.vega-int.ru

Received February 04, 2025 Revised February 14, 2025 Accepted April 07, 2025

Using the method of mesoscopic fluorescence molecular tomography (FMT), a phantom with a fluorophore forming periodic spatial structures was experimentally reconstructed. It is shown that the use of reflectance geometry with a high density of sources and detectors helps increase reconstruction accuracy and resolve structures 0.55 mm in diameter at depths to 5 mm inclusive. The depth sensitivity of the proposed mesoscopic FMT method was tested through the analysis of sensitivity functions obtained in a series of calculations by the modernized TurbidMC code that implements the Monte Carlo method. Calculated results demonstrate that the depth sensitivity can be improved due to the optical clearing of the object's surface layer.

Keywords: fluorescence molecular tomography, mesoscopic mode, sensitivity function, phantom with fluorophore, periodic spatial structure, reconstruction accuracy, depth sensitivity.

DOI: 10.61011/EOS.2025.05.61645.23-25

Introduction

In recent years, fluorescence molecular tomography (FMT) has become quite widespread as a molecular imaging method used to solve problems in experimental oncology [1,2]. As you know, the low spatial resolution is the "sticking point" in diffusion imaging. One of the ways to improve resolution is to switch from the macroscopic data recording mode to the mesoscopic mode [3,4], in which sources and detectors are located at small distances from each other (up to 10 mm) and relatively small areas of interest are restored (on the order of $10 \times 10 \times 10 \text{ mm}^3$). This transition allowed the researchers to finally achieve the desired submillimeter resolution for FMT images [5,6]). However, the transition to the mesoscopic mode is inevitably associated with an increased anisotropy of light scattering and a deterioration in the depth sensitivity of the FMT method. Therefore, the relevant question is what depths are available for reproducing fluorescent structures using mesoscopic FMT.

In the last few years, the authors of this paper have developed and partially investigated an original time-resolved FMT method based on an asymptotic approximation of the fluorescence source function [7–11]. A special feature of the proposed FMT method is that it is potentially capable of reconstructing the spatial distributions of not only the fluorophore absorption coefficient (or fluorophore concentration), but also the distributions of the fluorescence lifetime.

This parameter is particularly appreciated by researchers in the field of experimental oncology and fluorescent imaging, as it is resistant to changes in fluorescence intensity when measured on living objects, is highly sensitive to changes in the molecular environment of fluorescent biosensors, and provides important information about the processes occurring in tumor tissues at the molecular level [12–14]. The theory of the proposed mesoscopic FMT method is described in Ref. [8]. The case of macroscopic FMT was studied in Refs. [7,8] using numerical experiments. The program TurbidMC, which implements the Monte Carlo method, is described in Ref. [10]. This program is used for modeling fluorescence signals and calculating sensitivity functions for mesoscopic FMT. Some preliminary results of these studies are analyzed in Ref. [11]. The first physical experiment on the reconstruction of a phantom with a fluorophore is described in Ref. [9]. In this experiment, the mesoscopic data recording mode was used for the first time. It was possible to correctly restore the distributions of the fluorophore absorption coefficient and the fluorescence lifetime. However, the fluorophore was located at a depth of up to 4 mm and was a cylinder of relatively large diameter (3 mm), which did not allow us to draw any definite conclusions about either the spatial resolution of the method or its depth sensitivity. Thus, the relevant question is whether our method is capable of reproducing submillimeter-sized fluorescent structures at depths of more than 4 mm. To answer this question, an experiment was

30 465

conducted to reconstruct a phantom with a fluorophore forming periodic spatial structures. This paper describes the experiment and presents its results. Since they turned out to be worse than expected, a number of additional calculations were required to assess the potential for improving the accuracy of reconstruction and the depth sensitivity of the mesoscopic FMT method. The results and analysis of these calculations are also presented in this paper.

Reconstruction problem setup

A variant of the mesoscopic FMT method, which was used in Ref. [9], assumed a two-step approach to solving the reconstruction problem. In the first step, the so-called fluorescence parameter distribution function is restored, which contains both the distribution of the fluorophore absorption coefficient and the distribution of the fluorescence lifetime. In the second step, these distributions are separated by solving an overdetermined system of equations. the separation stage introduces additional errors into the reconstruction results, and given the complexity of the task set in this paper, it was decided at this stage of research to limit the reconstruction to only the distribution of the fluorophore absorption coefficient. In this case, the lifetime of fluorescence was assumed to be an a priori set constant. Thus, the mesoscopic FMT method used in this work is as follows. The reconstruction problem is reduced to the inversion of the Fredholm linear integral equation of the first kind:

$$p(\mathbf{r}_s, \mathbf{r}_d, t) = k \int_V W(\mathbf{r}_s, \mathbf{r}_d, \mathbf{r}, t) \mu_{af}(\mathbf{r}) d^3r$$
 (1)

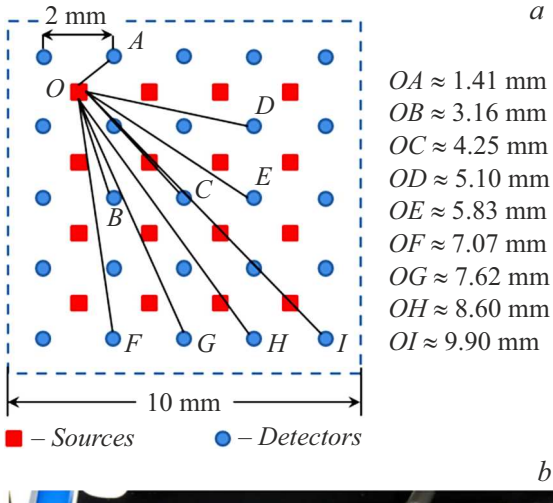
for the unknown distribution of the fluorophore absorption coefficient $\mu_{af}(\mathbf{r})$. In formula (1) $p(\mathbf{r}_s, \mathbf{r}_d, t)$ is the timeresolved fluorescence signal (Fluorescence Temporal Point Spread Function, FT-PSF) excited by an instantaneous source at point \mathbf{r}_s at time $t_s = 0$ and recorded at point \mathbf{r}_d at time t, k is the dimensionless proportionality coefficient, $W(\mathbf{r}_s, \mathbf{r}_d, \mathbf{r}, t)$ is the sensitivity function calculated using the TurbidMC program [10] and representing a 3D-distribution of weighting coefficients for a given source—detector link (SD link). The following expression is valid in our case for the coefficient k

$$k = \frac{4Dc\gamma}{\tau v^2 + 4Dc},\tag{2}$$

where D and c are the photon diffusion coefficient and the speed of light in the medium at the wavelength of exciting radiation, γ is the fluorescence quantum yield, τ is a priori value of the fluorescence lifetime, ν is the average velocity of the center of mass of the instantaneous distribution of photons along their average trajectory [8,15].

Next, equation (1) is discretized as it is described, for example, in Ref. [8], and the inverse problem is reduced to solving the system of linear algebraic equations

$$\mathbf{W}\boldsymbol{\mu} = \mathbf{p},\tag{3}$$



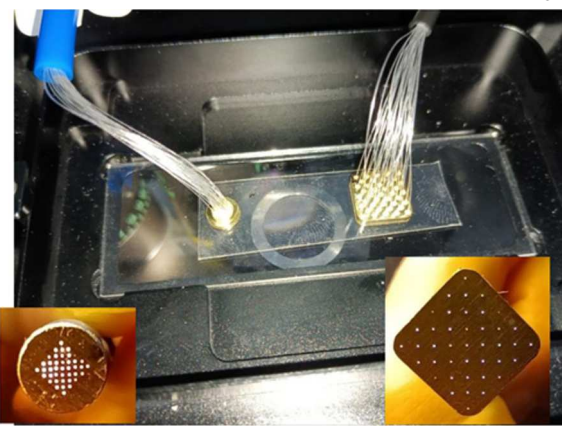


Figure 1. Geometry of data recording and values of all the different distances between sources and detectors (a), photo of the probe (left — setup side, right — phantom side) (b).

where $\mathbf{W} \equiv \{W_{i,j}\}_{1,1}^{IJ}$ is the sensitivity matrix, which contains discrete transposed sensitivity functions calculated for all I SD links involved in reconstruction; $\boldsymbol{\mu} \equiv \{\mu_j\}_1^J$ is a vector describing the desired distribution $\mu_{af}(\mathbf{r})$; $\mathbf{p} \equiv \{p_i\}_1^J$ is a vector of measurement data into which the results of processing the experimentally measured fluorescent temporal responses (FTR) are recorded.

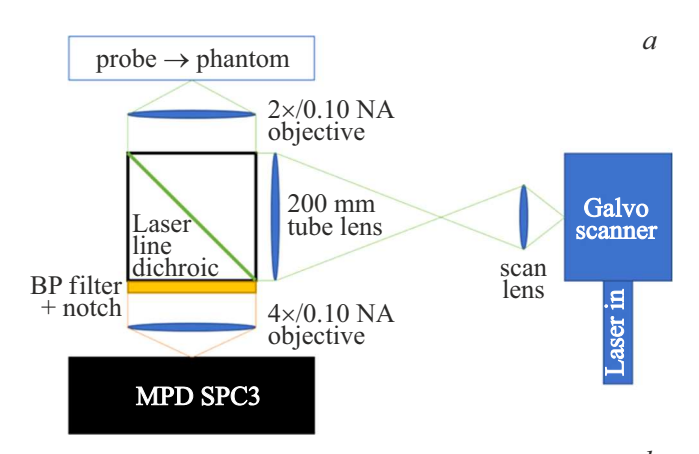
Since system (3) is obtained, as a rule, strongly underdetermined, optimization algorithms with regularization are used to solve it, for example, algorithms based on compressed sensing theory [16]. ART-FIST algorithm (algebraic reconstruction technique with fast iterative shrinkage thresholding) is chosen in this paper to solve (3), combining the Gordon algebraic reconstruction [17] and the fast iterative shrinkage-thresholding algorithm of Beck and Teboulle [18]. The algorithm is described in detail in Ref. [8] and has proven its efficiency in the reconstruction of sparse fluorescent tomograms.

Experiment and data preprocessing

An experiment on scanning a phantom with a fluorophore was conducted at the Research Center of Biotechnology

RAS (Moscow, Russia). In the experiment, a reflectance geometry was used with a scheme of the location of the input points of exciting radiation (sources) and the output points of fluorescence (detectors), as shown in Fig. 1, a. The figure on the right shows the values of all the different distances between the sources and the detectors for which the sensitivity functions were calculated. According to this scheme, a probe was developed containing 41 fibers with a core diameter of 100 µm OKM-UV-100/110/150-170 NA 0.22 (STC Fiber-Optic Devices, Russia), fixed in two holders. A photo of the probe is shown in Fig. 1, b.

The fluorescence tomography setup was designed using ThorLabs optomechanical units (USA), an LDH D-TA-560B PicoQuant laser (Germany), and a KineFLEX QiOptiq optical fiber light guide (UK), GVSM002 Thorlabs galvanometer (USA), SL50-CLS ThorLabs Scan Lens, TTL200-A ThorLabs Tube Lens, Di03-R488/561-t1-25 × 36 Semrock dichroic mirror (USA), HQ585/40 and ZET561NF emission filters (Chroma, USA), 2 × /0.10 NA PlanApo lens (Nikon, Japan), SPC3 avalanche photodiode array (Micro Photon Devices, Italy) and $4 \times /0.1$ NA Plan Achromat lens (Nikon, China). It can be noted that detection systems such as SPC3 are increasingly being used in fluorescence imaging and lifetime spectroscopy [19]. The scheme of the experimental FMT setup is shown in Fig. 2, a, and its image is shown in Fig. 2, b.



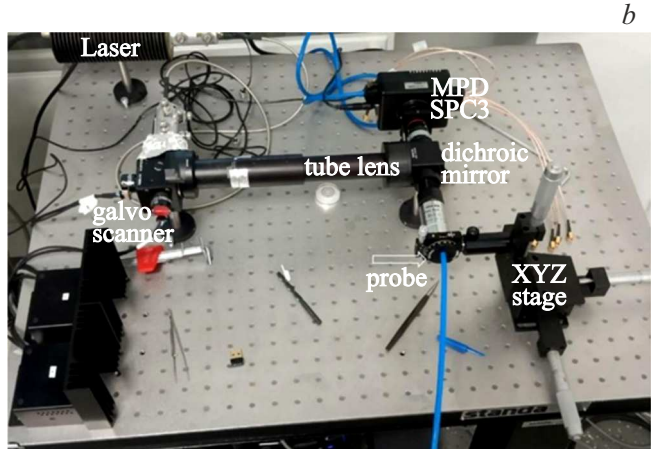


Figure 2. Experimental setup scheme (a) and its general photo (b).

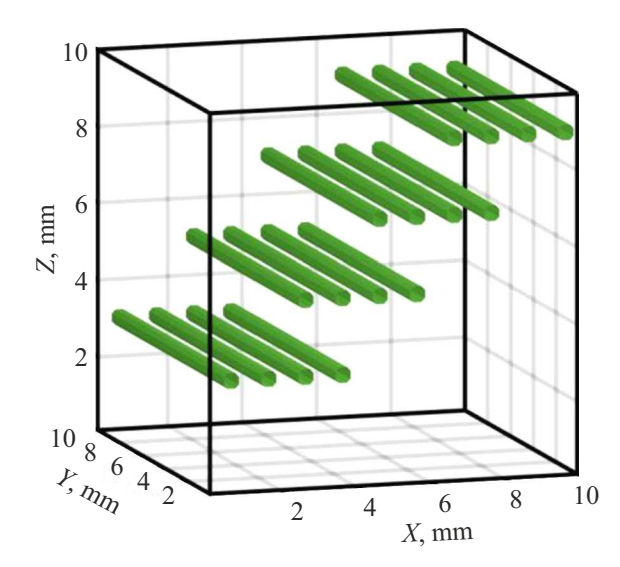


Figure 3. Area of reconstruction of the phantom with the size of $10 \times 10 \times 10 \,\mathrm{mm}^3$, containing periodic spatial structures.

The mating part of the optical probe was placed in the focal plane of the phantom for introducing the exciting radiation into optical fibers and recording the fluorescent signal, fixing the probe in a 3-position micrometer slide with a rotating holder. The centers of the cores of each optical fiber were aligned with the points of light input and output in accordance with the scheme of Fig. 1, a.

Silicone Sylgard 184 (Dow Corning, USA) with a mass fraction of TiO₂ 0.13% was chosen as the material of the phantom. In order to adequately calculate the sensitivity functions, measurements of the optical parameters of the phantom sample were performed at the Saratov National Research State University named after N. G. Chernyshevsky (Saratov, Russia): absorption coefficient, scattering coefficient, reduced scattering coefficient, scattering anisotropy factor and refractive index. First, diffuse reflection and total transmission spectra of the sample were recorded in the spectral range of 500-700 nm with a step width of 2 nm using Lambda 950 spectrophotometer (Perkin Elmer, USA). Then, the collimated transmission spectrum of the sample was recorded using USB4000-Vis-NIR fiber-optic spectrometer (Ocean Optics, USA) in the same spectral range. The diffuse reflection, collimated, and total transmission spectra of the phantom sample were used to calculate the spectral dependences of the absorption coefficient, the scattering anisotropy factor, and the reduced scattering coefficient using the inverse adding-doubling method [20]. refractive index of the phantom sample was measured using Abbe DR-M2/1550 multiwave refractometer (Atago, Japan) at a wavelength of 589 nm. The scattering coefficient μ_s of the sample was determined using the expression [21]

$$\mu_s' = \mu_s(1-g),\tag{4}$$

where μ'_s is the reduced scattering coefficient, g is the scattering anisotropy factor.

Values	of	optical	parameters	of	the	phantom	and	fluorescence
parameters								

Parameter	Value
Phantom absorption coefficient, mm ⁻¹	0.09
Phantom scattering coefficient, mm ⁻¹	1.82
Phantom scattering anisotropy factor	0.45
Phantom refractive index	1.43
Phantom absorption coefficient, mm ⁻¹	0.17
Fluorophore scattering coefficient, mm ⁻¹	0
Quantum yield of fluorescence	0.48
Fluorescence lifetime, ps	2200

Holes with a diameter of 0.55 mm were formed in the phantom to be filled with a solution with fluorophore so that the fluorophore formed periodic spatial structures at depths of 3, 5, 7, and 9 mm. The reconstruction area with the size of $10 \times 10 \times 10 \text{ mm}^3$ with periodic spatial structures is shown in Fig. 3. The fluorescent protein TagRFP with a concentration corresponding to an absorption coefficient of 0.17 mm⁻¹ (wavelength of 561 nm) was selected as the fluorophore. The fluorescence parameters of this fluorophore are listed on the website [22]. wavelengths of excitation (561 nm) and emission (585 nm) are very close, and it is sufficient to obtain rough estimates of the parameters (with an error of about 15%) for calculating the sensitivity functions, the same values of the optical parameters of the phantom and the fluorescence parameters were used for both wavelengths, which are given in the table.

The preprocessing of the measured FTR was performed using the MATLAB package according to the algorithm described in [9], and consisted in noise compensation of each FTR and its deconvolution with the instrumental response, also measured in the experiment, in order to evaluate the FT-PSF. To compensate for noise, the Savitsky—Golay filter [23] was used, implemented in MATLAB by the operator sgolayfilt (·) . Deconvolution of smoothed FTR with instrumental response was performed using the accelerated Lucy—Richardson algorithm [24], which has proven its efficiency in processing both one-dimensional signals and images. This algorithm is implemented in the MATLAB package by the operator deconvlucy(·). Then for each the *i*th FT-PSF resulted, we calculated

$$p_i = \int_0^{t_d} \Phi \mathbf{B} \Phi \mathbf{P} T_i(t) dt, \qquad (5)$$

where t_d is the time of "cutoff" of pulse along the leading edge (the detector delay time). It was the values of (5) that were written into the measurement data vector \mathbf{p} .

Calculation and analysis of sensitivity functions

A phantom with a certain structural filling with a fluorophore, different from the real phantom, was numerically defined for calculating the ten sensitivity functions for the distances shown in Fig. 1, a. Just like the real phantom (Fig. 3), the numerical phantom had periodic structures at the same depths of 3, 5, 7, and 9 mm. But these structures were formed not by cylinders, but by parallelepipeds with a square cross-section with the size of $0.5 \times 0.5 \,\mathrm{mm}^2$. In addition, the row at each depth consisted of not four, but five structures. This was done intentionally in order to artificially set a certain "error" when using a priori knowledge. Thus, a priori information was used only about the depths of the structures, but not about their exact shape and location. The sensitivity functions were calculated not for the cube of $10 \times 10 \times 10 \,\text{mm}^3$ (the selected size of the reconstruction area), but for the parallelepiped of $18 \times 10 \times 12 \,\mathrm{mm}^3$. In this case, the source and detector were located at an equal distance from the center of the face z = 0 of the parallelepiped. This was done to attain the most complete understanding of distribution features for not only short but also long SD links.

The calculations were performed using the TurbidMC program on a multiprocessor computing facility of Zababakhin All-Russia Research Institute of Technical Physics (Snezhinsk, Russia). Each calculation considered from 10^9 to 10^{10} histories, each of which began by introducing an excitation photon into a numerically specified phantom and continued by modeling its trajectory, as well as the trajectories of the fluorescent photons generated by it. All trajectories were simulated until the photon's weight decreased to a given value (in our case 10^{-12}). The time for one calculation of this series was 10-15 h.

As examples, the results of calculations of sensitivity functions for the shortest (1.41 mm) and longest (9.9 mm) SD-link are shown in Fig. 4 as 3D distributions of the weighting coefficients. Visual analysis of 3D images in Fig. 4 shows that the obtained distributions have extensive sparse zones and are very far from smooth functions. This suggests the need to improve the statistical accuracy of calculations. In order to pre-evaluate the potential possibility of reproducing various layers of periodic spatial structures of the phantom during reconstruction using the calculated sensitivity functions, the following sequence of actions was performed. First, each SD link in Fig. 1, a was assigned its own sensitivity function. Moreover, this was done, of course, for the cube of size 10x10x10 mm³. Secondly, all sensitivity functions were summed up and a 3D picture of the distribution of the sum over the reconstruction area was obtained (Fig. 5, a), as well as cross-sections of this distribution at the depths of the periodic structures (Fig. 5, b-e). It can be seen from Fig. 5 that the space is well filled in the case of depths 3 and 5 mm (Fig. 5, b, c), it is worse at a depth of 7 mm (Fig. 5, d), the distribution becomes sparse at a depth of 9 mm (Fig. 5, e). Thus,

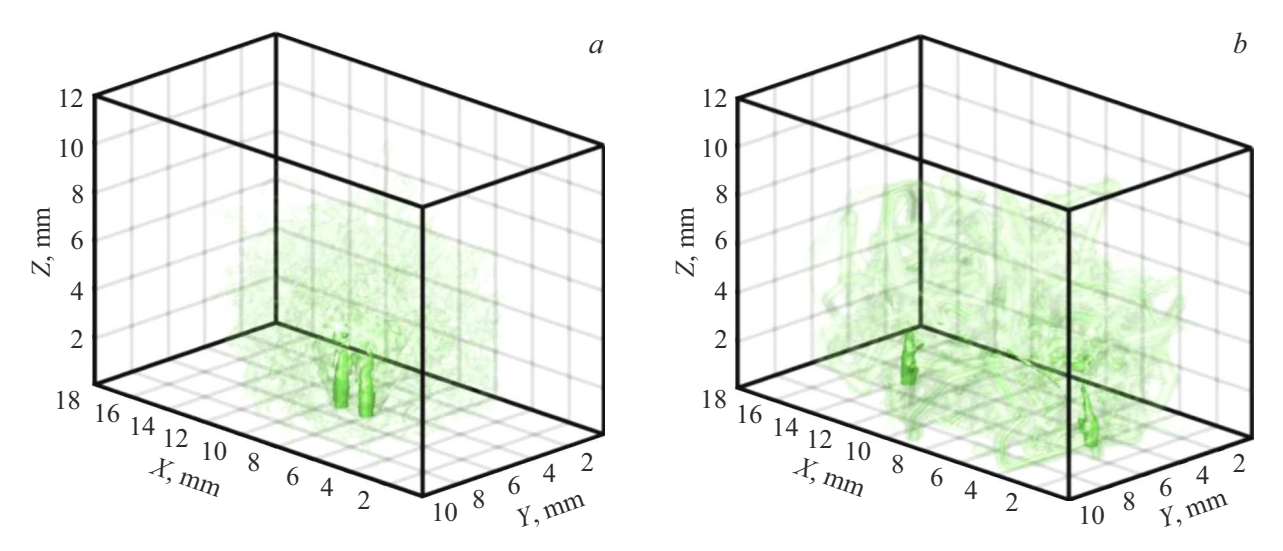


Figure 4. 3D images of sensitivity functions calculated for two distances between the source and the detector: 1.41 (a), 9.9 mm (b).

even before the reconstruction, it became clear that serious problems could arise with reproducing structures at depths of 7 and 9 mm.

Reconstruction results

The reconstruction area with the size $10 \times 10 \times 10 \text{ mm}^3$ was restored, the voxel size was set to 0.1 mm. Thus, the number of voxels and, accordingly, columns of the sensitivity matrix W was equal to J = 1000000. The number of SD links and rows of the matrix was $I = 16 \times 25 = 400$. As mentioned above, the ART-FIST algorithm described in detail in Ref. [8] was used for reconstruction. algorithm parameters were also selected according to how it was proposed in the same paper. The reconstruction results are shown in Fig. 6. Fig. 6, a shows a 3D image. Figures 6, b-e demonstrate 2D sections of a 3D image at depths of 3, 5, 7, and 9 mm of periodic structures. Here and further, the image palettes are graded in inverse millimeters. It can be seen that structures at a depth of 3 mm are reproduced with distortion (Fig. 6, b). Only fragments of structures are visible at the depth of 5 mm (Fig. 6, c). Depths of 7 and 9 mm were generally unavailable for reproduction (Fig. 6, d, e). Quantitative image quality characteristics such as the correlation coefficient [25] and the deviation factor [26] are calculated for 2D images shown in Fig. 6, b, c. The obtained values are 0.7965 and 0.6207 for the image of Figure 6(b) and 0.6051 and 0.8695 for the image of Figure 6(c), respectively. These values also indicate the unsatisfactory quality of the recovered CT scans. Thus, the following issues have become relevant. Is it possible to improve the quality of reproduction of structures at depths of 3 and 5 mm? Is it possible to make depths of 7 and 9 mm available for reproduction?

About possibilities for improving reconstruction accuracy

The first thing that was done to answer the questions was to check the correctness of the preprocessing of the measured FTR and the formation of a vector of measurement data **p**. For this purpose, a numerical experiment was set up that exactly repeated the physical experiment. For this purpose, a numerical experiment was set up that exactly repeats the physical experiment. The reconstruction results turned out to be very close to those shown in Fig. 6. Thus, the issue turned out to be not the correctness of the preprocessing of experimental data, but something else.

Then two hypotheses were put forward. The first is the insufficient density of sources and receivers (indeed, the number of links $16 \times 25 = 400$ turned out to be relatively small). The second is the unsatisfactory statistical accuracy of the calculation of sensitivity functions. Another numerical experiment was performed to test the first hypothesis, in which the number of sources and detectors was increased by 4 times. This was done as follows. The geometric system of Fig. 1, a shifted in its plane first by 1 mm horizontally, then by 1 mm vertically, and finally by $\sqrt{2}/2$ mm diagonally. Thus, three more geometric systems (or subsystems) were formed, which were combined with the original into a new geometry. The new geometry of the sources and detectors resulted in 4 times more, i.e. 64 and 100, respectively. As for the SD links only the links within each of the subsystems were used, the links of sources and detectors between different subsystems were not involved in the reconstruction. This made it possible to avoid additional time-consuming calculations of sensitivity functions. As a result, in the new geometry, the number of SD-links was also 4 times greater than in the geometry of Fig. 1, a.

As a result, 4 times more SD links were obtained in the new geometry than in the geometry of Fig.1, a. It follows

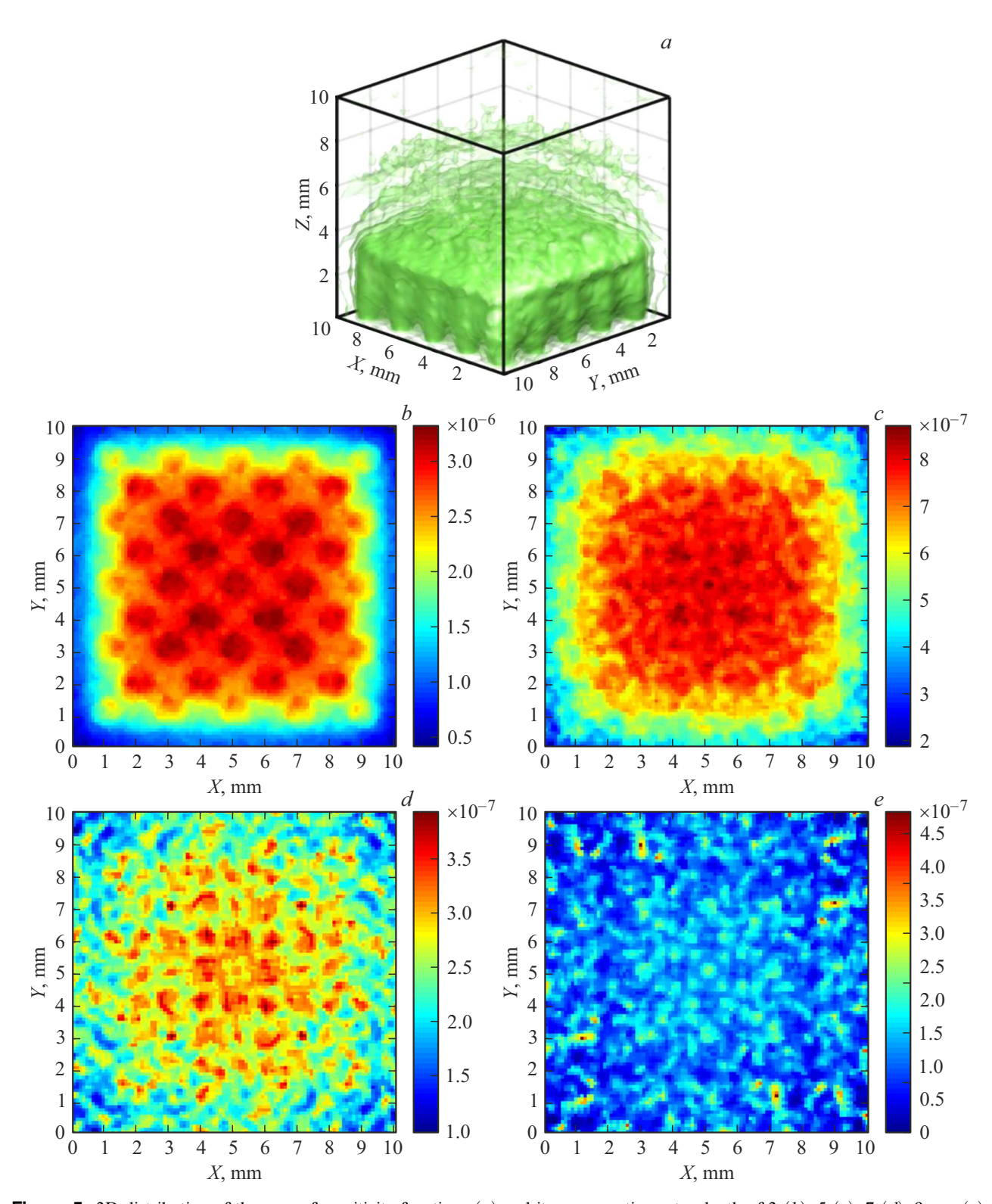


Figure 5. 3D distribution of the sum of sensitivity functions (a) and its cross-sections at a depth of 3 (b), 5 (c), 7 (d), 9 mm (e).

from the visual analysis of Fig. 7 that it was possible to significantly improve the quality of reproduction of periodic structures at depths of 3 and 5 mm (Fig. 7, *b*, *c*, respectively). It can be seen that the cylinders of the structures are well resolved relative to each other. The obtained gain in

reconstruction accuracy is also evidenced by the values of the correlation coefficient and the deviation factor calculated for the images in Fig. 7, b, c: 0.9117 and 0.2114 for the image of Fig. 7,b and 0.8643 and 0.3338 for the image of Fig. 7,c. But the structures at depths of 7 and 9 mm

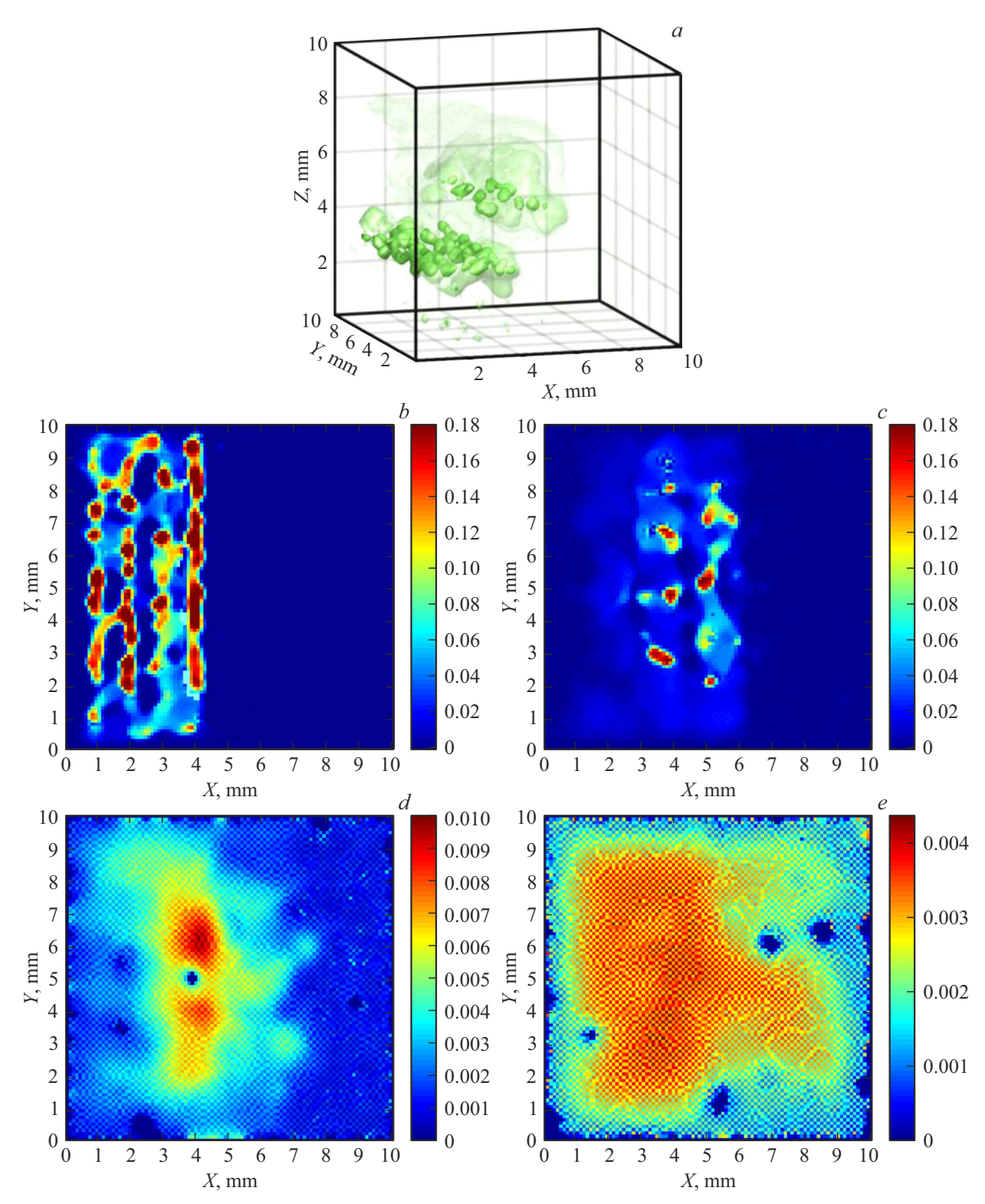


Figure 6. The results of reconstruction of periodic spatial structures: 3D image (a) and its 2D sections at the depths of the structures of 3 (b), 5 (c), 7 (d), 9 mm (e).

still could not be reproduced (Fig. 7, d, e). Thus, it was possible to show that the use of "high density geometry" can significantly improve the accuracy of reconstruction of structures at depths of 3 and 5 mm, but still does not

improve the depth sensitivity of the proposed method of mesoscopic FMT.

As for the hypothesis about the unsatisfactory statistical accuracy of calculating sensitivity functions, the results

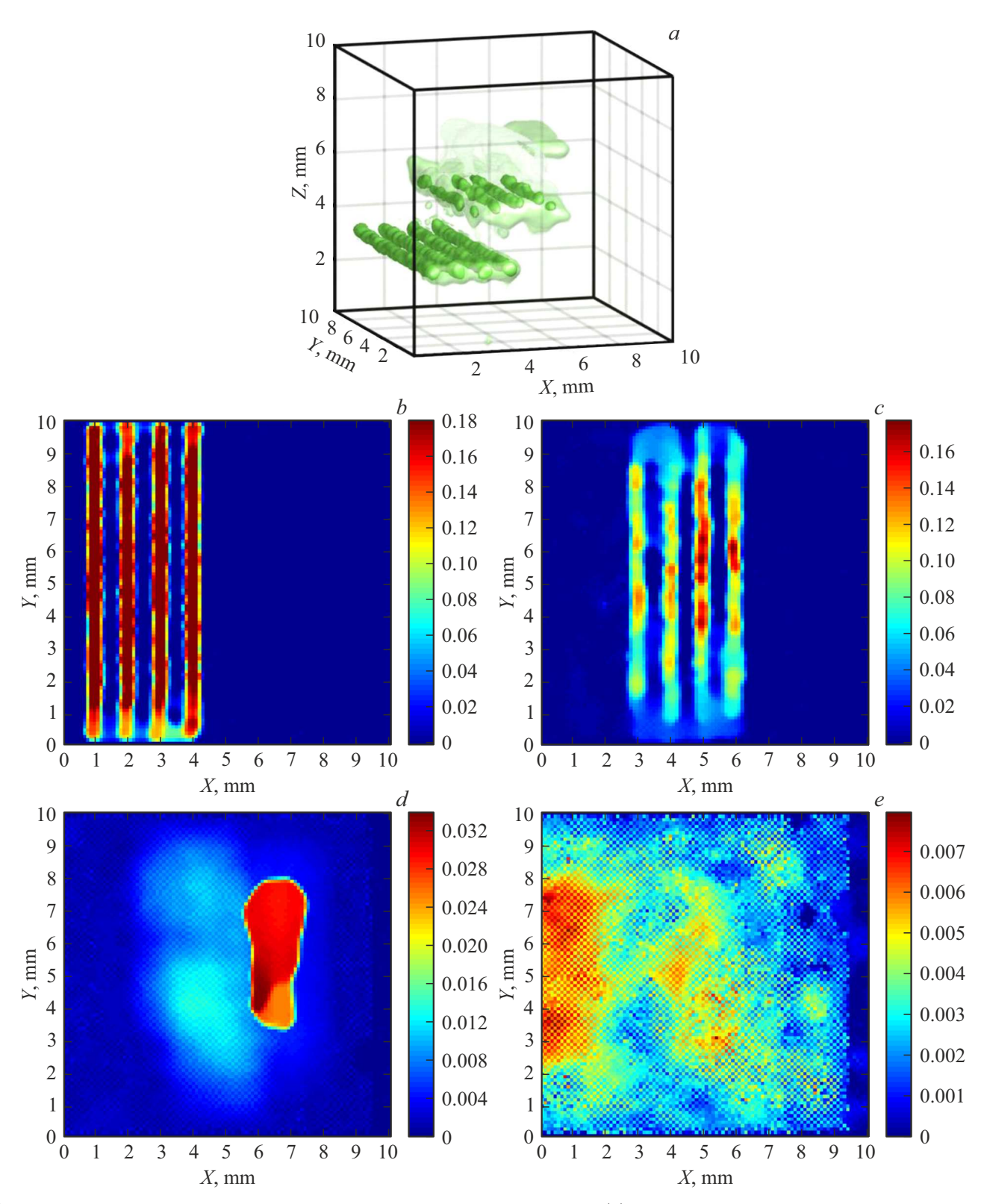


Figure 7. Reconstruction results for the case of high-density geometry: 3D image (a) and its 2D sections at the depths of the structures of 3 (b), 5 (c), 7 (d), 9 mm (e).

shown in Fig. 4–6 clearly indicate the need to increase it. There were several ways to go. We were particularly interested in the Gardner method [27], according to which

not only the forward calculation of the sensitivity function is performed, but also the adjoint one. In the adjoint calculation, the detector is placed in the position of the source, and the source is placed in the position of the detector. Then a superposition of two calculations is performed — forward and adjoint. The calculation examples presented in Ref. [27] show that it is possible to obtain an almost smooth sensitivity function.

At the present stage of research, it was decided to take a different way and modernize the TurbidMC program by introducing an artificial process of δ -scattering. The δ -scattering process is characterized by the introduction of a coefficient μ_{δ} for this "fictitious" interaction, the magnitude of which is determined by the probability of the formation of a fluorescent photon in the body of the fluorophore. The path length l is selected from the distribution

$$p(l) = \mu_t \exp(-\mu_t l) \tag{6}$$

with attenuation coefficient $\mu_t = \mu_a + \mu_s + \mu_\delta$, where μ_a and μ_s are absorption and scattering coefficients, respectively. The weight of a photon after interaction in a medium is calculated using the formula

$$\omega_{k+1} = \omega_k \frac{\mu_s + \mu_\delta}{\mu_t}. (7)$$

If the interaction occurs in a fluorophore, then a weight is assigned to the fluorescent photon.

$$\omega_{k+1}^{flu} = \omega_k \frac{\mu_a}{\mu_t}.$$
 (8)

In this case, the scattering process is divided into two processes: normal scattering and δ -scattering, which are randomly selected according to the probabilities $\mu_s/(\mu_s+\mu_\delta)$ and $\mu_\delta/(\mu_s+\mu_\delta)$, respectively. The choice of the value μ_δ does not affect the values of the calculated quantitates, but it does affect the variance of the estimated values, and therefore the statistical error of the estimated value. The choice of μ_δ depends on the specific conditions of the problem and is related to the characteristic size of the fluorophore inclusions d by the expression

$$\mu_{\delta} \approx \frac{1}{d} - (\mu_a + \mu_s). \tag{9}$$

Such an upgrade of the TurbidMC program has improved the statistical accuracy of sensitivity function calculations. Some of the calculation results for the upgraded program are given in the next section.

Possible ways to increase the depth sensitivity

Sensitivity functions were calculated in this experiment taking into account a priori knowledge of the depths of periodic structures with fluorophore. As a result, not entirely satisfactory results were obtained. What if we change the conditions for calculating sensitivity functions appropriately? One of the options is the calculation for a scattering phantom without a fluorophore — the case of

diffusion optical tomography at the wavelength of exciting radiation. It is proved in Refs. [28,29] that the calculations of the sensitivity function for an object with and without a fluorophore are virtually identical if the absorption coefficients of the object and the fluorophore are close (in our case, this is not entirely true, since the absorption coefficient of the fluorophore is almost twice the absorption coefficient of the phantom (see Table)). Another option for changing the calculation conditions is to assume that the fluorophore occupies the entire reconstruction area. However, in this case, it will be necessary to artificially set some non-zero scattering for the fluorophore, otherwise such a calculation makes no sense at all. It should be noted that such an option has not yet been substantiated by anyone, and so far it seems problematic to adapt the proposed method of mesoscopic FMT to it. Nevertheless, to test the hypothesis of a likely increase in depth sensitivity, three calculations were performed using the modified TurbidMC program for the three model scattering media presented above. The sensitivity comparison criterion for different calculations was the depth of "penetration" of the sensitivity function inside the object.

Figure 8 shows three sensitivity functions (more precisely, their effective 2D cross-sections with a plane passing through the centers of the source and detector) calculated using the modernized program. The distance between the source and the detector is 5 mm, and the depth of the object (the height of the images of the figure) is 8, a shows the calculation result using a priori information about the depths of the structures. It was also considered during the experiment. In contrast to Fig. 4, Fig. 8, a shows the structures themselves they are clearly visible at a depth of 3 mm and barely noticeable at a depth of 5 mm. This means that it has indeed been possible to improve the statistical accuracy of calculations by introducing a fictitious δ -scattering process into the program. In this case, the depth of penetration of the sensitivity function into the object can be estimated as \sim 6 mm. Fig. 8, b shows the calculation result for an object without a fluorophore. Unfortunately, the penetration depth was ~ 4 mm. Therefore, this calculation method cannot be an alternative to Fig. 8, a. Fig. 8, c shows the calculation results for an object that is a fluorophore with a scattering coefficient two times lower than the scattering coefficient of objects in the two previous calculations. With respect to the penetration depth, the best result was obtained at ~ 7 mm. Thus, despite the fact that the conditions of the latter calculation are somewhat artificial and currently not fully justified, it makes sense to think about the possibility of adapting the mesoscopic FMT method to such a calculation of the sensitivity function.

Another possible way to increase depth sensitivity is to use optical clearing of the surface layer of the object. The effect of optical clearing on depth sensitivity was evaluated using the simplest model, according to which the value of the scattering coefficient in the layer from the surface to a depth of 1 mm of the phantom was reduced by 2 times.

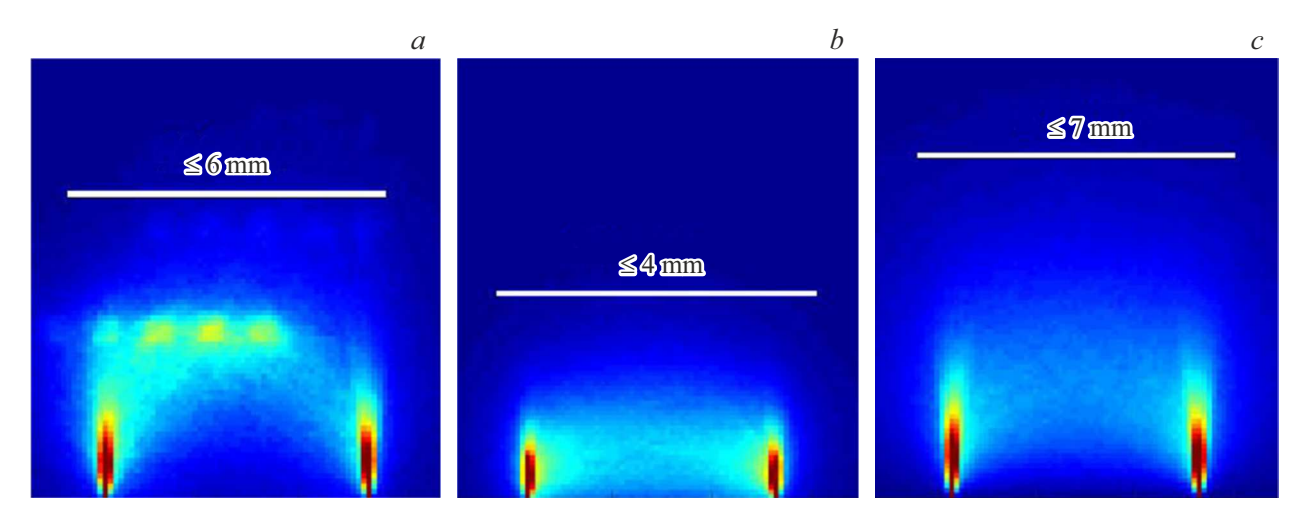


Figure 8. The results of calculations of sensitivity functions: with a priori knowledge of the depths of the fluorophore (a), an object without a fluorophore (b), an object is a fluorophore with a scattering coefficient reduced by 2 times (c).

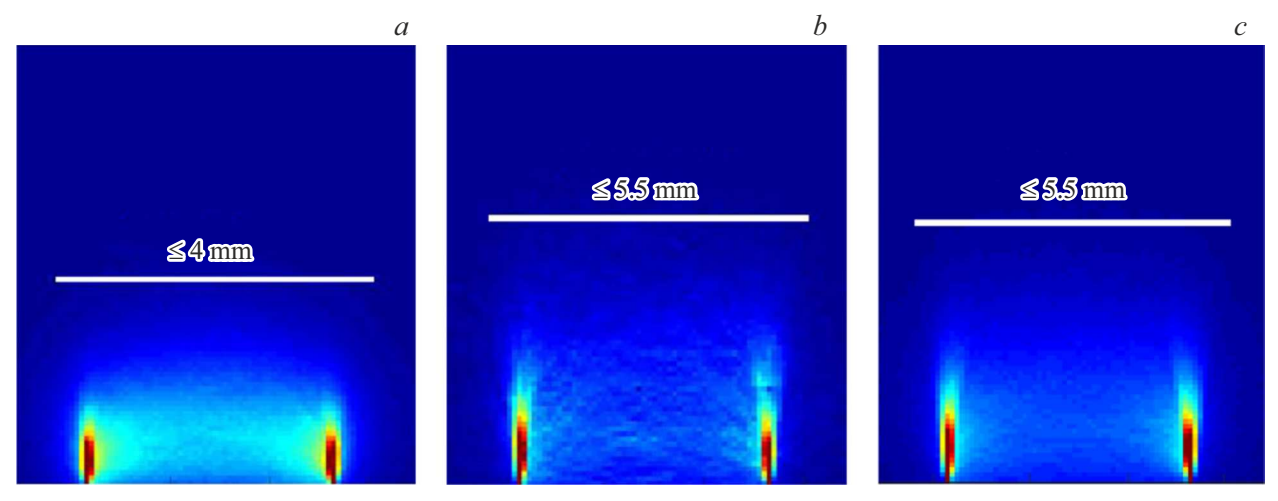


Figure 9. The results of calculations of sensitivity functions: an object without clearing (a), the surface layer with a thickness of 1 mm (b) is cleared, the entire object is cleared (c).

It is proved in Refs. [30,31] that such modification of optical properties of biological tissue is practically achievable through the use of clearing agents. In this case, the agent's duration is calculated in tens of minutes. Thus, two more calculations of sensitivity functions were performed using the upgraded TurbidMC program. All calculations were performed for a scattering object without a fluorophore. The visualization of the image of Fig. 8, b is repeated in Fig. 9, a, for convenience of visual comparison. Figure 9, b shows the calculation result for an object with a cleared surface layer with a depth of 1 mm. Finally, Fig. 9, c shows the calculation result for a fully cleared object (an almost impossible case, specially introduced for comparative analysis of the results). In the last two calculations, very similar sensitivity functions were obtained, the depth of penetration into the object was $\sim 5.5 \, \text{mm}$ in both cases. This is a very interesting result, which can be explained by the fact

that it is the surface layer where the photons carrying information about the object [32] are redistributed, and which nevertheless requires confirmation in an experiment on the reconstruction of a phantom with fluorophore. Of course, only experiment will give an answer to the question - whether structures will be reproduced at a depth of at least 7 mm under the condition of optical clearing of the surface layer. But since the depth of 5.5 mm is definitely greater than 4 mm (Fig. 9, a, b), it can already be safely argued that optical clearing is a reliable way to increase the depth sensitivity of the FMT method.

Conclusion

An experiment has been performed in this study to reconstruct a phantom with a fluorophore forming periodic spatial structures at various depths using mesoscopic FMT. The experimental results are presented and discussed, as well as the results of a numerical experiment for the geometry of a high density of sources and receivers. It is shown that the use of high-density geometry is a reliable method for improving the accuracy of reconstruction. In this case, structures with a diameter of 0.55 mm can be reliably resolved at depths up to and including 5 mm. Thus, it is advisable to use only such geometry in subsequent physical experiments. The paper also discusses ways to increase the depth sensitivity of the mesoscopic FMT method. One way is the selection of optimal conditions for calculating sensitivity functions. At the moment, this way has only been identified and requires additional research. Another way is the optical clearing of the surface layer of the scattering object. This way is justified in this paper by calculations of sensitivity functions for an object without a fluorophore. Of course, the next step is to verify this way by experimenting with the reconstruction of a phantom with a fluorophore, which is the goal of the upcoming research. It is also necessary to further search for ways to improve the statistical accuracy of sensitivity function calculations, which is very important for obtaining high-quality reconstructions of fluorescent images.

The work was supported by the Ministry of Higher Education and Science of the Russian Federation, grant No. 13.2251.21.0009 (Agreement No. 075-15-2021-942). The work of Savitsky A.P. was carried out within the framework of the state assignment of the Federal Research Center of Biotechnology of the Russian Academy of Sciences.

Conflict of interest

The authors declare that they have no conflict of interest.

References

- C. Darne, Y. Lu, E.M. Sevick-Muraca. Phys. Med. Biol., 59
 R1 (2014). DOI: 10.1088/0031-9155/59/1/R1
- [2] Y. An, K. Wang, J. Tian. Visual Comput. Industry Biomed. Art., 1, 1(2018). DOI: 10.1186/s42492-018-0001-6
- [3] A. Dunn, D. Boas. Opt. Lett., 25 (24), 1777 (2000).DOI: 10.1364/OL.25.001777
- [4] E.M.C. Hillman, D.A. Boas, A.M. Dale, A.K. Dunn. Opt. Lett., 29(14), 1650 (2004). DOI: 10.1364/OL.29.001650
- [5] F. Yang, M.S. Ozturk, L. Zhao, W. Cong, G. Wang, X. Intes. IEEE Trans. Biomed. Eng., 62 (1), 248 (2015). DOI: 10.1109/TBME.2014.2347284
- [6] S. Gao, M. Li, J.T. Smith, X. Intes. Biomed. Opt. Express., 13(9), 4637 (2022). DOI: 10.1364/BOE.460216
- [7] A.B. Konovalov, V.V. Vlasov. Proc. SPIE, 11457, 1145703 (2020). DOI: 10.1117/12.2560139
- [8] A.B. Konovalov, V.V. Vlasov, A.S. Uglov. Int. J. Numer. Meth. Biomed. Eng., 37(1), e3408 (2021). DOI: 10.1002/cnm.3408
- [9] A.B. Konovalov, V.V. Vlasov, S.I. Samarin, I.D. Soloviev, A.P. Savitsky, V.V. Tuchin. J. Biomed. Opt., 27(12), 126001 (2022). DOI: 10.1117/1.JBO.27.12.126001

- [10] S.I. Samarin, A.B. Konovalov, V.V. Vlasov, I.D. Solovyov,A.P. Savitsky, V.V. Tuchin. Comput. Opt., 47 (5), 673 (2023)(in Russian). DOI: 10.18287/2412-6179-CO-1295
- [11] A.B. Konovalov, V.V. Vlasov, S.I. Samarin, A.S. Uglov, I.D. Solovyov, A.P. Savitsky, V.V. Tuchin. In: Novel Technologies in Medicine, Biology, Pharmacology and Ecology. Materials of the conference NT+ME'23 (Gurzuf, 2023) P. 161 (in Russian). DOI: 10.47501/978-5-6044060-3-8.161-169
- [12] T.S. Blacker, Z.F. Mann, J.E. Gale, M. Ziegler, A.J. Bain, G. Szabadkai, M.R. Duchen. Nat. Commun., 5, 3936 (2014). DOI: 10.1038/ncomms4936
- [13] M. Lukina, A. Orlova, M. Shirmanova, D. Shirokov, A. Pavlikov, A. Neubauer, H. Studier, W. Becker, E. Zagaynova, T. Yoshihara, S. Tobita, V. Shcheslavskiy. Opt. Lett., 42(4), 731 (2017). DOI: 10.1364/OL.42.000731
- [14] E.A. Shirshin, M.V. Shirmanova, A.V. Gayer, M.M. Lukina, E.E. Nikonova, B.P. Yakimov, G.S. Budylin, V.V. Dudenkova, N.I. Ignatova, D.V. Komarov, V.V. Yakovlev, W. Becker, E.V. Zagaynova, V.I. Shcheslavskiy, M.O. Scully. Proc. Natl. Acad. Sci. USA., 119(9), e2118241119 (2022). DOI: 10.1073/pnas.2118241119
- [15] V.V. Lyubimov, A.G. Kalintsev, A.B. Konovalov, O.V. Lyamtsev, O.V. Kravtsenyuk, A.G. Murzin, O.V. Golubkina, G.B. Mordvinov, L.N. Soms, L.M. Yavorskaya. Phys. Med. Biol., 47(12), 2109 (2002).
 DOI: 10.1088/0031-9155/47/12/308
- [16] A.B. Konovalov. Physica Medica, 124, 104491 (2024). DOI: 10.1016/j.ejmp.2024.104491
- [17] R. Gordon, R. Bender, G.T. Herman. J. Theor. Biol., 29(3), 471 (1970). DOI: 10.1016/0022-5193(70)90109-8
- [18] A. Beck, M. Teboulle. SIAM J. Imaging Sci., **2**(1), 183 (2009). DOI: 10.1137/080716542
- [19] J.L. Lagarto, C. Gredi, F. Villa, S. Tisa, F. Zappa, V. Shcheslavskiy, F.S. Pavone, R. Cicchi. Sensors, 19, 2678 (2019). DOI: 10.3390/s19122678
- [20] S.A. Prahl, M.J.C. van Gemet, A.J. Welch. Appl. Opt., 32(4), 559 (1993). DOI: 10.1364/AO.32.000559
- [21] Multimodal Optical Diagnostics of Cancer. Ed. by V.V. Tuchin, J. Popp, V. Zakharov (Springer, Cham, 2020). DOI: 10.1007/978-3-030-44594-2
- [22] The fluorescent protein TagRFP [electronic resource]. URL: https://www.fpbase.org/protein/tagrfp
- [23] S.J. Orfanidis. *Introduction to Signal Processing* (Prentice-Hall, Englewood Cliffs, New Jersey, 1996).
- [24] D.S.C. Biggs, M. Andrews. Appl. Opt., 36(8), 1766 (1997). DOI: 10.1363/AO.36.001766
- [25] Z. Wang, A.C. Bovik, H.R. Sheikh, E.P. Simoncelli. IEEE Trans. Image Process., 13(4), 600 (2004). DOI: 10.1109/TIP.2003.819861
- [26] B. Moulden, F.A.A. Kingdom, L. Gatley. Perception, 19(1), 79 (1990). DOI: 10.1068/p190079
- [27] A.R. Gardner, C.K. Hayakawa, V. Venugopalan. J. Biomed. Opt., 19(6), 065003 (2014). DOI: 10.1117/1.JBO.19.6.065003
- [28] J. Chen, V. Venugopal, X. Intes. Biomed. Opt. Express., **2**(4), 871 (2011). DOI: 10.1364/BOE.2.000871
- [29] X. Jiang, Y. Deng, Z. Luo, K. Wang, L. Lian, X. Yang, I. Meglinski, Q. Luo. Opt. Express, 22(26), 31948 (2014). DOI: 10.1364/OE.22.031948

- [30] Handbook of Tissue Optical Clearing: New Prospects in Optical Imaging. Ed. by V.V. Tuchin, D. Zhu, E.A. Genina (Ration Taylor & Francis Group LLC, CRC Press, Boca, 2022). DOI: 10.1201/9781003025252
- [31] D.K. Tuchina, I.G. Meerovich, O.A. Sindeeva, V.V. Zherdeva, A.P. Savitsky, A.A. Bogdanov Jr, V.V. Tuchin. J. Biophotonics, 13(11), e201960249 (2020). DOI: 10.1002/jbio.201960249
- [32] X. Yang, T. Jiang, L. Liu, X. Zhao, X. Yu, M. Yang, G. Liu, Q. Luo. J. Innov. Opt. Health Sci., 16(1), 2330002 (2023). DOI: 10.1142/S1793545823300021

Translated by A.Akhtyamov